Sensors and Materials, Vol. 36, No. 1 (2024) 177–189
MYU Tokyo

S & M 3508

Charge-Sharing Detection Method Using Semiconductor Detectors with Different Electron and Hole Mobilities

Toshiyuki Takagi,[1,2*] Katsuyuki Takagi,[2,3] Junichi Nishizawa,[2,3]
Hisashi Morii,[2] Hiroki Kase,[3] Kento Tabata,[3] and Toru Aoki[2,3]

[1]Graduate School of Medical Photonics, Shizuoka University,
3-5-1 Johoku, Naka-ku, Hamamatsu 432-8011, Japan
[2]ANSeeN Inc., 3-1-7 Wajiyama, Naka-ku, Hamamatsu 432-8003, Japan
[3]Research Institute of Electronics, Shizuoka University, 3-5-1 Johoku, Naka-ku, Hamamatsu 432-8011, Japan

(Received September 7, 2023; accepted November 20, 2023)

Keywords: radiation detector, semiconductor detector, charge sharing, cadmium telluride

The significance of X-ray spectral information is steadily growing. However, pile-up is becoming a pertinent problem at high dosage levels. Additionally, attempts to mitigate pile-up by reducing the surface area of the detector result in charge sharing, making accurate spectrum determination complicated. When materials such as cadmium telluride are employed as detectors, a significant disparity in the mobility of electrons and holes can lead to pulses in the opposite direction across multiple electrodes. We propose to identify charge-sharing events by detecting these opposing pulses. We found that eliminating events associated with negative pulses from the spectrum reduced the full width at half maximum of the peak from 15.9 to 14.4 keV. The proposed method improves the accuracy of spectral measurements under high flux to reduce the effect of charge sharing in single-point spectral measurements.

1. Introduction

X-ray spectral information plays a crucial role in flux calculations,(1) dual-energy material decomposition,(2) artifact correction,(3) and the performance evaluation and calibration of X-ray detectors.(4) Spectral measurements necessitate the evaluation of each X-ray photon. However, pile-up presents a formidable challenge under high-flux conditions, such as in medical computed tomography (CT), impeding accurate measurement. Therefore, the spectrum is obtained via simulation or spectral reconstruction.(5,6)

Pile-up is the phenomenon wherein the signal from a photon incident on the detector overlaps with the signal from another photon before the information processing of the initial photon has been concluded, thus preventing the accurate determination of photon count and energy. The probability of pile-up increases with radiation flux, reflecting the augmented influx of photons onto the detector. An effective strategy to counteract the consequences of pile-up involves reducing the area of the detector and the influx of incident radiation photons.(7) However, charge sharing becomes problematic with decreasing electrode area. Charge sharing entails the splitting

*Corresponding author: e-mail: takagi.toshiyuki.19@shizuoka.ac.jp
https://doi.org/10.18494/SAM4654

ISSN 0914-4935
https://myukk.org/

of electron–hole pairs generated within the detector between neighboring electrodes.[8,9] This results in increased counts of detected photons and the detection of lower photon energy, both of which increase the difficulty of obtaining the correct spectrum.

Coplanar grid detectors[10] and 2D array detectors for X-ray imaging[11,12] exemplify instances where the effect of charge sharing on the output signal from the detector is considered. Coplanar grid detectors adopt the output waveform profile of each electrode. This technique involves adding or subtracting these outputs to obtain the desired output. Conversely, 2D array detectors are designed to add the signals of neighboring pixels when they are detected simultaneously. Both methods necessitate spectral assessments across multiple electrodes, effectively spanning the entire electrode area.

When solely measuring the X-ray spectrum at a single point, the practice of calculating multiple outputs, as observed in the aforementioned detectors, is undesirable because it increases the electrode area of the detector and accentuates the effect of pile-up. However, adopting strategies to mitigate charge sharing at all electrodes is not necessary, unlike the case of pixel detectors. One plausible approach involves a simplified configuration featuring a single-pixel signal electrode on one side of the detector and auxiliary electrodes arranged for charge-sharing correction near the signal electrode. In this case, the auxiliary electrode does not require spectral measurement, unlike the signal electrode, thus enabling reductions in charge-sharing effects. Additionally, independent nuclear instruments module (NIM) bins or benchtop instruments can be allocated to multiple electrodes, akin to coplanar grid detectors, facilitating waveform analysis while performing measurements.

Incident photons on detectors equipped with multiple electrodes yield signals of opposing polarities at adjacent electrodes.[13–15] This phenomenon is associated with situations where the incident location of the photon lies near the electrode boundary. The mobilities of the electrons and holes in the detector differ significantly. In addition, there are instances where one of the carriers lags within the detector. The fact that there is an incident photon near the boundary indicates that a charge-sharing event that splits the electron cloud must be included in this negative pulse event.

In this study, we propose a method of reducing the effects of charge sharing. The proposed approach entails fabricating a semiconductor-based detector, such as cadmium telluride (CdTe), characterized by marked electron and hole mobility discrepancies.[16] This detector incorporates dedicated electrodes for signal detection and correction (hereafter called SIG and AUX, respectively). The strategy involves detecting negative pulses generated across neighboring electrodes concurrently with normal signals.

2. Data, Materials, and Methods

2.1 Characteristic-shaped signal generated in CdTe detector: generating negative pulses

Upon the ingress of X-ray photons into a semiconductor detector under a high applied voltage, the photoelectric effect generates electron–hole pairs. Of these newly formed electron–hole pairs, electrons traverse towards the anode and holes traverse towards the cathode. In this

process, the energy of the X-ray photons manifests as an electrical signal, perceptible by quantifying the charge induced by this movement. The speed of electrons and holes propagating within the semiconductor is governed by their mobility and the prevailing electric field strength. In the case of CdTe, the electron mobility surpasses the hole mobility by approximately 10.[9] This difference results in the emergence of a signal with a two-stage slope (see Fig. 1; electrons with a higher mobility have a larger slope and holes with a lower mobility have a smaller slope). Furthermore, the shape of the signal depends on the position of the generated electron–hole pair. When an electron–hole pair is generated at the center of the detector thickness (Fig. 1), the signal is equally affected by electrons and holes. In contrast, electron–hole pair generation near the anode leads to a signal predominantly governed by holes. Conversely, if a pair is generated near the cathode, the signal predominantly reflects the behavior of electrons (Fig. 2).

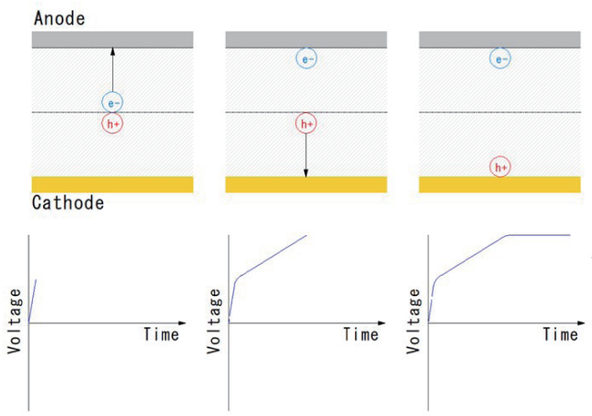

Fig. 1. (Color online) Signal when electron–hole pairs are generated at the center of the detector thickness.

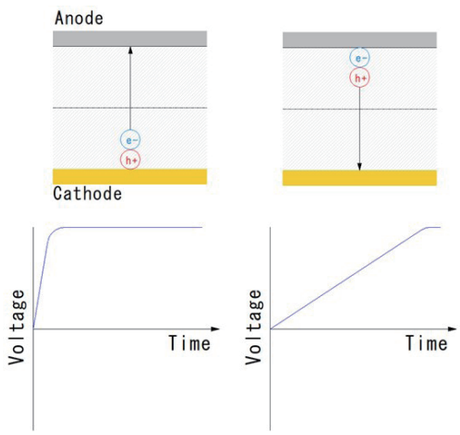

Fig. 2. (Color online) Signals when electron–hole pairs are generated near the cathode and anode of the detector.

The morphology of the waveform resulting from the interaction of X-ray photons with the detector and the occurrences affecting charge sharing and multielectrode phenomena during the signal output process have been summarized in a paper on coplanar grid detectors.[4] As mentioned above, the shape of the waveform is intrinsically linked to the detector's spatial distribution of electron–hole pairs. A characteristic pulse that differs from the usual pulse can be generated using a semiconductor such as CdTe as the detector material, which has very different electron and hole mobilities. If electron–hole pairs are generated near the boundary of the electrodes and span the region from the center of the thickness to the anode, distinctive pulses are generated, characterized by opposite positive and negative sides (negative pulses). The mechanism underpinning the generation of negative pulses is described in the following.

The process of generating a negative pulse is illustrated in Fig. 3. Electron–hole pairs are generated by incident X-ray photons in the CdTe detector. Electrons move faster than holes owing to their higher mobility, resulting in a positive pulse in the SIG. The movement of electrons disrupts the electrical balance inside the semiconductor owing to the holes remaining at the center. The effect of the remaining holes extends to the neighboring electrode because the electron–hole pairs are generated near the electrode boundary (AUX in Fig. 3). Hence, negative charges (electrons) are injected from the outside into the electrodes of the AUX to maintain the electrical balance. The injected electrons are detected as a signal, generating a negative pulse at the AUX. Subsequently, the effect of hole movement becomes dominant after the electrons reach the electrode. A signal with a small slope appears in the SIG owing to the movement of the holes. As the holes move, the electrical balance in CdTe returns to normal, prompting the release of the previously injected electrons into the correcting electrode. Finally, as holes reach the electrode, signal fluctuations cease concurrently across both the signal and the AUX.

Figure 4 illustrates a case where electron–hole pairs are generated near the center of the detector thickness, resulting in marginal charge sharing. This configuration generates a positive signal in the SIG and a negative signal in the AUX, similar to the case of Fig. 3. However, a positive signal component originating from the split electrons is generated in the AUX and canceled out by the negative pulse. Consequently, the amplitude of the negative pulse generated in the AUX is smaller than that in shared generated events, reducing the signal in the SIG owing to its division. Furthermore, the conclusion of signal variations in the AUX extends the baseline, culminating in a positive position.

2.2 Calculating signal generation probability

We calculated the approximate probability of the detector generating a negative pulse. The occurrence of such a negative pulse depended on the specific location within the detector where the electron–hole pair was generated. A negative pulse was observed when an electron–hole pair was generated near the boundary of the electrodes and at a depth ranging from the anode to the center of the detector. ^{137}Cs was primarily responsible for emitting gamma rays at 662 keV; however, these gamma rays might enter the detector with lower-energy photons owing to scattering or other factors. In this study, we exclusively considered 662 keV photons. The size of the charge cloud generated by the detector depends on the photon energy. For 662 keV photons, the mean diameter of the charged cloud was 220 μm.[17] The relationship between the detector

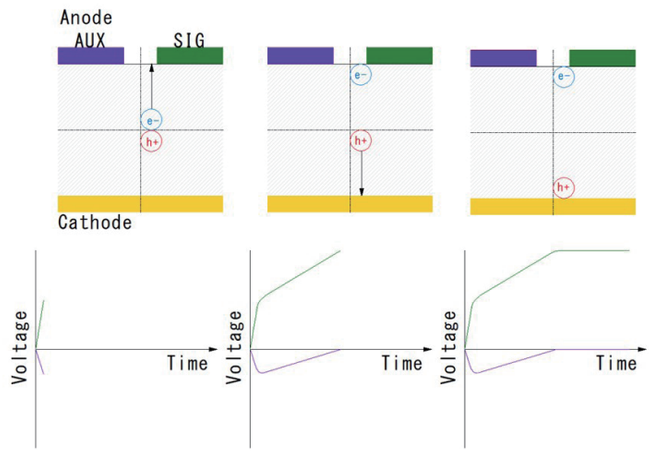

Fig. 3. (Color online) Process of events where a negative pulse is generated at the correcting electrode.

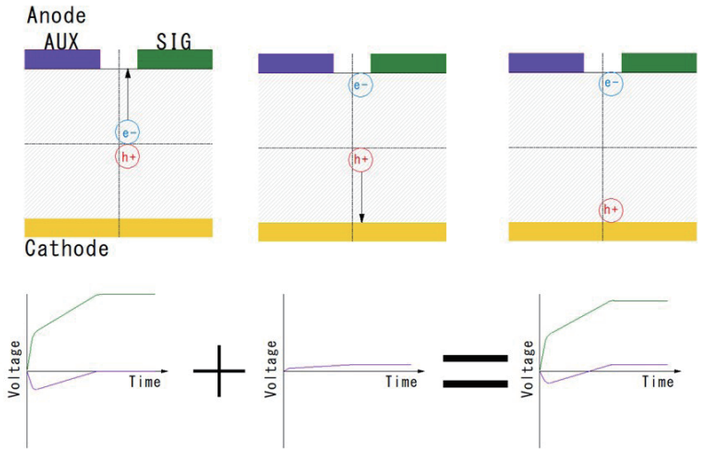

Fig. 4. (Color online) Event in which a negative pulse is generated in the AUX and the charge cloud is slightly split.

and the charge cloud is shown in Fig. 5. We estimated that a negative pulse was generated at the AUX when the charge cloud was generated in the area ranging from the electrode boundary to a distance of 110 μm (the radius of the charge cloud) on the SIG side, extending from the anode to the thickness center. This region encompassed approximately 5.5% of the entire detector area. However, if a charge cloud is generated immediately below the electrode boundary, the absence of negative signal components and negative pulses may not be generated. Moreover, the greater the distance of the carrier from the electrode, the greater the relative effect on the correcting electrode, with the effect extending beyond the 110 μm threshold on the SIG side. Owing to these factors, the measured probability of negative pulses can deviate from 5.5%.

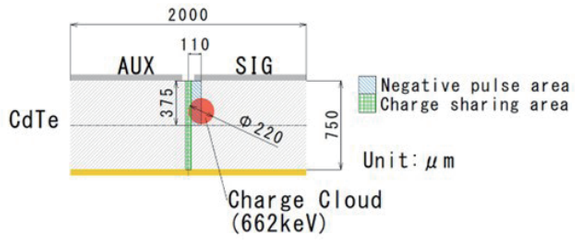

Fig. 5. (Color online) Cross section of the CdTe detector from the side, illustrating the area where a negative pulse is generated.

2.3 Measurement method

Multiple electrodes were attached to the CdTe semiconductor, enabling the measurement of the radiation spectrum and negative pulses across each electrode. The detector and the measurement system are shown in Figs. 6 and 7, respectively. CdTe (measuring 2 × 2 × 0.75 mm^3) provided by Acrorad Co., Ltd. was employed as the detector material. Two electrodes of the same size (2 × 0.95 mm^2) were attached to the CdTe surface with a gap of 0.1 mm between them (the electrodes were labeled as SIG and AUX). The anode of the detector (both SIG and AUX) was subjected to a voltage of 200V. ^{137}Cs was used as the radiation source. Each electrode was connected to a CSP02 charge-sensitive preamplifier (ANSeeN Inc.), a 4419HI waveform-shaping amplifier (CLEAR-PULSE Inc.), a ZMCAN-CH04-01 waveform analyzer (ANSeeN Inc.) as a multichannel analyzer (MCA), and an oscilloscope to measure the spectrum and pulse. This MCA can record timestamps of all events, enabling the detection of events coinciding with negative pulses, and the time constant of the preamplifier is 100μs. The spectrum was measured with the SIG triggered positively and the AUX triggered negatively, because the MCA could choose to trigger positively or negatively while measuring the signal. Additionally, the rise time of the signal was measured to determine the position of electron–hole generation. The output of the preamplifier was used for the measurements. The rise time of the signal, t_r (s)—the time required for the carriers to move in the semiconductor—can be obtained from the equation

$$t_r = dt / \mu V , \tag{1}$$

where d is the distance traveled by the carriers (cm), t corresponds to the thickness of the detector (cm), μ denotes the mobility (cm^2/Vs), and V represents the voltage (V). Employing the detector parameters, namely, μ_e = 1100 (cm^2/Vs), μ_h = 100 (cm^2/Vs),[16] V = 200 V, and t = 0.75 mm, we found that the rise time was approximately 26 ns for the shortest instances (pertaining to events where the electron–hole pairs were only affected by electrons produced near the anode). It increased to approximately 281 ns for the longest instances (corresponding to events primarily affected by holes generated near the cathode).

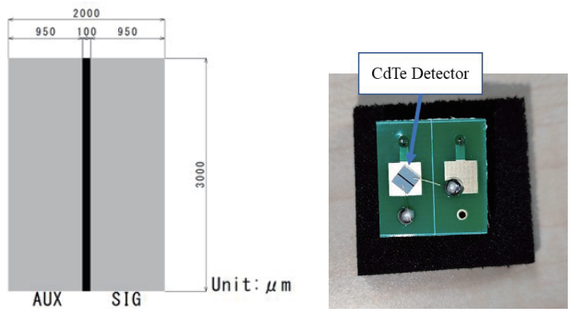

(a) (b)

Fig. 6. (Color online) (a) Top view of the fabricated CdTe detector and (b) photograph of the actual detector.

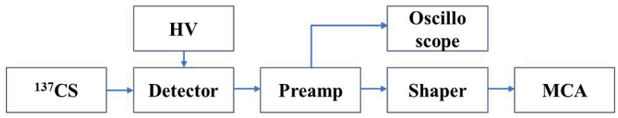

Fig. 7. (Color online) Measurement system.

3. Results

Figure 8 shows waveforms portraying negative pulse events of the preamplifier output captured via an oscilloscope. Channel 1 (yellow) corresponds to the SIG signal, whereas channel 2 (light blue) shows the AUX signal. The horizontal axis represents 100 ns/div in time and the vertical axis represents 50 mV/div for channels 1 and 2. The rising signal in channel 1 indicates a photon event due to gamma radiation from ^{137}Cs; it is a two-stage signal with fast- and slow-rising components due to electron and hole transfer processes, respectively. Simultaneously, the downward pulse in channel 2 encompasses the negative pulse event (see Sect. 2), consisting of a falling component due to electron transfer and a return to the baseline component due to hole transfer.

Figure 9 illustrates a negative pulse event with a slight charge cloud split of the preamplifier output, measured with an oscilloscope. Channels 1 (yellow) and 2 (light blue) correspond to the SIG and AUX signals, respectively. The horizontal axis represents 200 ns/div in time, whereas the vertical axis represents 50 mV/div for channels 1 and 2. The general shape of the waveform is the same as that in Fig. 8. However, the negative pulse in channel 2 did not return to the baseline even after the hole movement was completed. Moreover, the signal change ended at a position higher than the baseline owing to the effect of the split charge cloud.

Figure 10 shows a negative pulse event measured using an oscilloscope through a shaper. Channels 1 (yellow) and 2 (light blue) denote the SIG and AUX signals, respectively. The horizontal axis represents time (4 μs/div), whereas the vertical axis represents 100 mV/div for

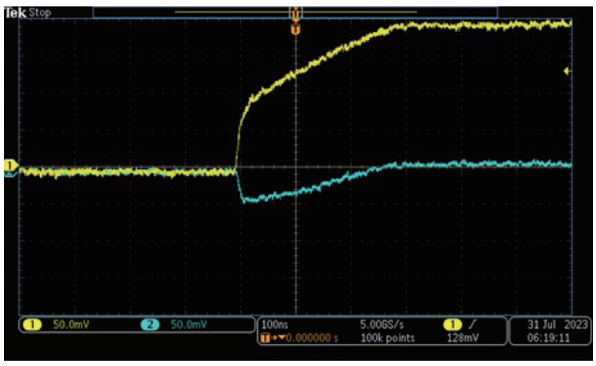

Fig. 8. (Color online) Oscilloscope capture of measured negative pulse events.

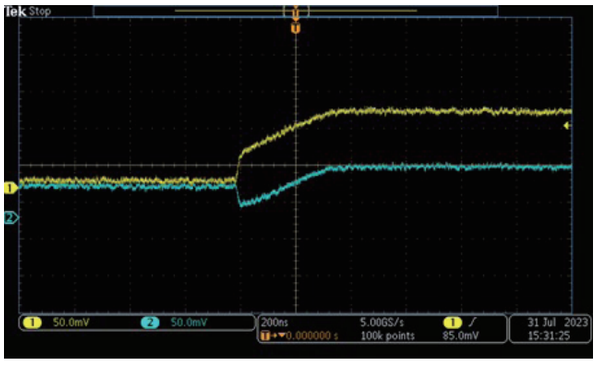

Fig. 9. (Color online) Oscilloscope capture of measured negative pulse event with slight change cloud split.

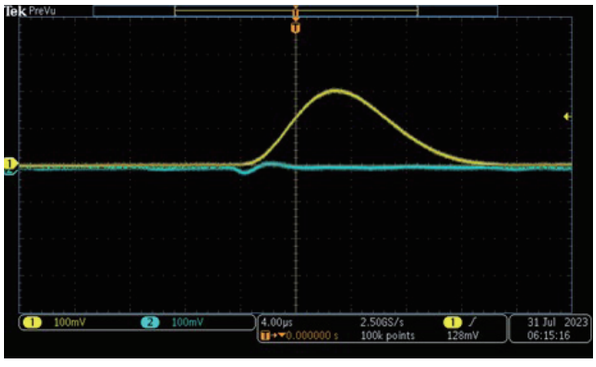

Fig. 10. (Color online) Oscilloscope capture of a negative pulse event measured through a shaper.

both channels. The constants of channels 1 and 2 were set to 2 and 0.5 μs, respectively, leading to signal shaping according to these settings. A negative pulse event was measured without problems, even after shaping.

Spectral measurements were undertaken with the SIG triggered positively and the AUX triggered negatively. Events detected simultaneously using the SIG and AUX were extracted and removed from the SIG spectrum. A comparison of the waveforms obtained before and after the event removal is shown in Fig. 11, with the expanded peak area depicted in Fig. 12. In both figures, the blue and orange curves represent the spectral observed before and after the event removal, respectively. The vertical axis represents the number of counts, whereas the horizontal axis represents the energy (keV). The full width at half maximum (FWHM) values of the photoelectric peaks were 15.9 and 14.4 keV, respectively. The percentage of events removed from the photoelectric peak was approximately 9%. Figure 13 shows the spectrum of the removed events. The peak energy of the removed events was 655.5 keV.

Figure 14 shows the distribution of the distance from the cathode at which electron–hole pairs were generated, calculated from the rise time measured at the preamplifier output of the SIG. The vertical axis represents the number of counts, whereas the horizontal axis represents the distance (mm) from the cathode where the electron–hole pairs originated. The blue waveform in Fig. 14 indicates the extracted photoelectric peak event, the orange waveform is the blue waveform with the negative pulse event removed, and the gray waveform indicates the removed events. The measured rise times were assigned to depths on the basis of their relationship with the drift times in Eq. (1), resulting in the distribution presented in Fig. 14. The negative values and the areas where the thickness of the detector exceeded 0.75 mm were due to the noise-induced blurring of the detected rise time.

4. Discussion

The waveforms in Figs. 8 and 9 depict negative pulse events (see Sect. 2). Significantly, the waveform in Fig. 9 shows a rising signal eventually exceeding the baseline while generating a negative pulse at the AUX, indicating the occurrence of charge sharing. Specifically, a charge-sharing event was detected by triggering a negative pulse event. Additionally, we showed that the energy resolution was improved by eliminating these events, irrespective of the presence or absence of charge sharing (see Fig. 12).

Following the verification of the rise time derived from the waveform in Fig. 8, we found that the travel time of the electrons was 26.5 ns, whereas that of the holes totaled 290 ns. These durations surpassed the assumptions made in Sect. 2. This divergence is attributed to the application of 200 V to the detector, which is lower than the customary measurement voltage, resulting in a non-uniform electric field within the detector and a decrease in carrier transfer rate.[18] However, an electron–hole pair event occurred at approximately half the detector depth, below the SIG, because the ratio of the signal component generated by electrons is the same as the ratio of the signal component generated by holes.. The depth at which the electron–hole pairs were generated was calculated from the measured rise time of the photoelectric peak of ^{137}Cs (Fig. 14). This evaluation indicated that electron–hole pairs were generated throughout the

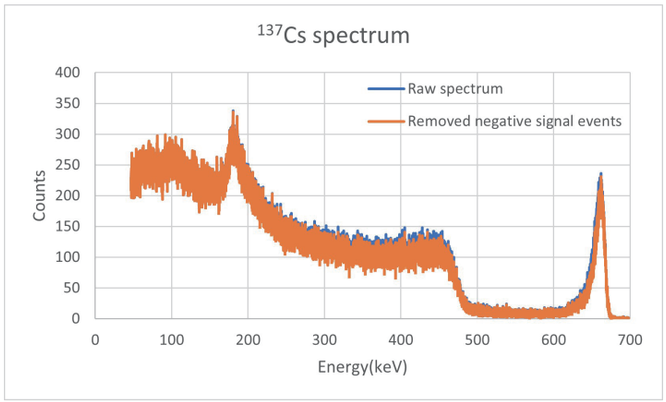

Fig. 11. (Color online) Comparison of the spectrum measured at the SIG and the spectrum from which the event detected coincided with the removal of the negative pulse.

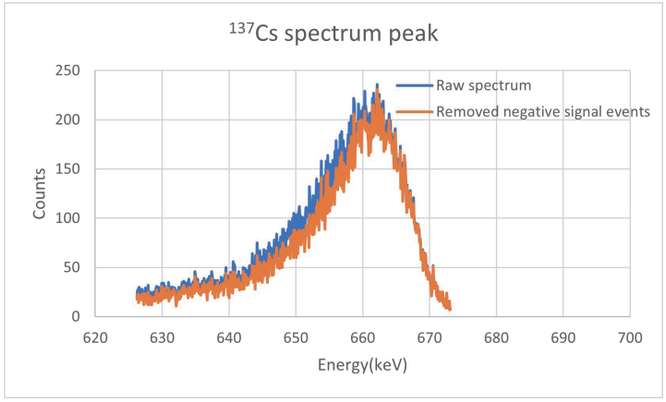

Fig. 12. (Color online) Expanded peak area of Fig. 11.

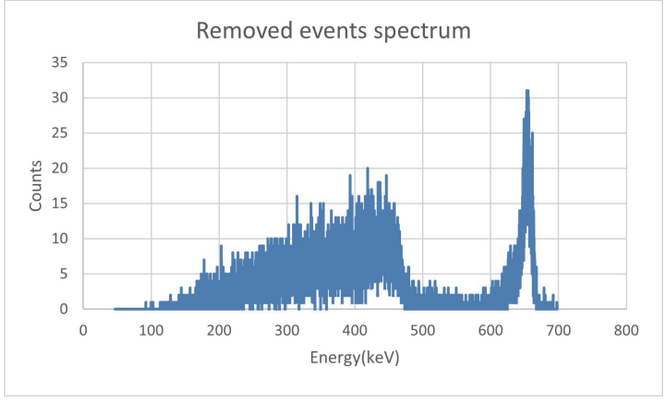

Fig. 13. (Color online) Spectrum of events removed from Fig. 11.

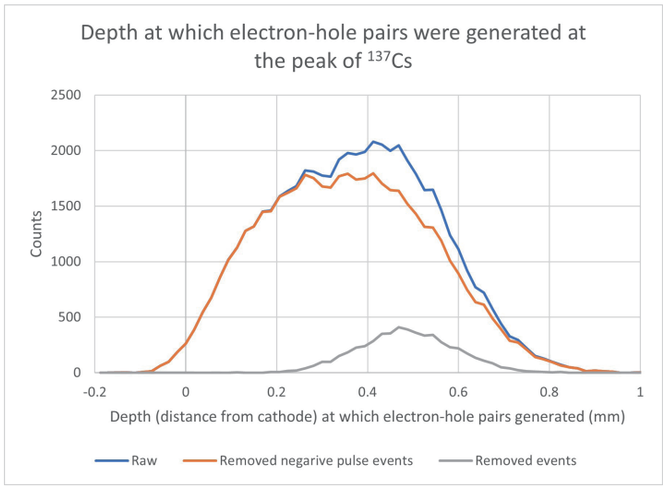

Fig. 14. (Color online) Distribution of the depth (distance from the cathode) at which electron–hole pairs were generated, calculated from the rise time of the signal at the peak of ^{137}Cs measured at the SIG.

detector, with the greatest number at the center of the detector. After removing the effect of noise from the distribution of removed events, the depth at which electron–hole pairs were generated was calculated to be approximately in the range of 0.26–0.71 mm.

The percentage of observed negative pulse events was approximately 9%, surpassing the estimated value of 5.5% (Fig. 12). This implies that the region in which negative pulse events occurred was wider than that under the trial condition. As previously outlined, the depth covered a range of 0.26–0.71 mm (0.45 mm), representing the region of negative pulse events with a 9% probability of negative pulse occurrence. The range from the electrode boundary to the SIG side was 0.15 mm. This indicates that the proposed method can detect negative pulse events up to the region where the ratio of the distance between the position of electron–hole pair generation and the signal electrode and that between the position of electron–hole pair generation and the correction electrode is 1:1.2.

5. Conclusions

A structure with a single-pixel SIG on one side of the detector and an auxiliary electrode for charge-sharing correction around the SIG has emerged as a viable option during X-ray spectral measurements conducted under high flux. In this case, the SIG must be used for spectral measurement. However, the auxiliary electrode does not partake in the spectral measurement process. This strategic allocation allows the potential impact of pile-up to be alleviated. Therefore, we demonstrated that when the mobilities of electrons and holes differ significantly, as in a CdTe detector, the detection of events involving charge sharing becomes feasible by detecting pulses opposing the direction of signals emanating from the output of multiple electrodes.

We designed a CdTe detector with two electrodes for signal detection (SIG) and correction (AUX). Employing a configuration where the SIG was positively triggered while the AUX was negatively triggered enabled the simultaneous measurement of a negative pulse spectrum and a standard spectrum. The analysis of SIG measurement results enabled the removal of the signal event generated at the SIG, whereas negative pulse events were detected at the AUX. Consequently, the energy counts lower than the photoelectric peak (662 keV) within the spectrum were eliminated. Moreover, the half width of the peak portion was reduced. Approximately 9% of counts were removed from the photoelectric peak portion (600–700 keV), surpassing the precalculated percentage of negative pulse generation. This discrepancy is likely due to a broader region of negative pulse occurrence on the SIG side than initially assumed during the trial calculation. The depth (distance from the anode) at which the electron–hole pairs were generated in the detector was confirmed from the signal's rise time. Negative pulses were generated when electron–hole pairs formed in the region from the center of the detector thickness to the anode.

A charge-sharing event detection method for spectral measurements under high flux was proposed and tested. The results indicate that the proposed method improves the accuracy of spectral measurements under high flux by reducing the effect of charge sharing in single-point spectral measurements.

Acknowledgments

Part of this research is based on the Cooperative Research Project of Research Center for Biomedical Engineering.

References

1 J. J. DeMarco, C. H. Cagnon1, D. D. Cody, D. M. Stevens, C. H. McCollough, J. O. 'Daniel, and M. F. McNitt-Gray: Phys. Med. Biol. **50** (2005) 3989. https://doi.org/10.1088/0031-9155/50/17/005
2 D. Lee, J. Lee, J. Mina, B. Lee, B. Lee, K. Oh, J. Kim, and S. Cho: Nucl. Instrum. Methods Phys. Res., Sect. A. **884** (2018) 105. https://doi.org/10.1016/j.nima.2017.12.009
3 W. Zbijewski, F. J. Beekman: IEEE. Trans. Med. Imaging. **25** (2006) 817. https://doi.org/10.1109/TMI.2006.872328
4 H-M. Cho, H. Ding, B. P. Ziemer, and S. Molloi: Phys. Med. Biol. **59** (2014) 7211. https://doi.org/10.1088/0031-9155/59/23/7211
5 G. Poludniowski, G. Landry, F. DeBlois, P. M. Evans, and F. Verhaegen:Phys. Med. Biol. **54** (2009) N433. https://doi.org/10.1088/0031-9155/54/19/N01
6 X. Duan, J. Wang, L. Yu, S. Leng, and C. H. McCollougha: Med. Phys. **38** (2011) 993 https://doi.org/10.1118/1.3547718
7 T. Flohr, M. Petersilka, A. Henning, S. Ulzheimer, J. Ferda, and B. Schmidt: Physica Med. **79** (2020) 126. https://doi.org/10.1016/j.ejmp.2020.10.030
8 C. Allwork, D. Kitou, S. Chaudhuri, P. J. Sellin, P. Seller, M. C. Veale, N. Tartoni, and P. Veeramani: IEEE Trans. Nucl. Sci. **59** (2012) 1563. https://doi.org/10.1109/TNS.2012.2195678
9 S. L. Bugby, K. A. Koch-Mehrin, M. C. Veale, M. D. Wilson, and J. E. Lees: Nucl. Instrum. Methods Phys. Res., Sect. A **940** (2019) 142. https://doi.org/10.1016/j.nima.2019.06.017
10 P. N. Luke: IEEE Trans. Nucl. Sci. **42** (1995) 207. https://doi.org/10.1109/23.467848
11 K. Taguchi: Med. Phys. **47** (2020) 2085. https://doi.org/10.1002/mp.14047
12 E. N. Gimenez, R. Ballabriga, M. Campbell, I. Horswell, X. Llopart, J. Marchal, K. J. S. Sawhney, N. Tartoni, and D. Turecek: J. Instrum. **6** (2011) https://doi.org/C01031.10.1088/1748-0221/6/01/C01031

13 I. Vasylchenko, R. Grill, E. Belas, P. Praus, and A. Musiienko: Sensors **20** (2020) 85. https://doi.org/10.3390/s20010085
14 G. F. Knoll: Radiation Detection and Measurement. (Wiley, New York, 2000) 3rd ed., pp. 789–794.
15 J. R. Macri, L.-A. Hamel, M. Julien, R. S. Miller, B. Donmez, M. L. McConnell, J. M. Ryan, and M. Widholm: IEEE Trans. Nucl. Sci. **51** (2004) 2453. https://doi.org/10.1117/12.551958
16 J. Fink, H. Krüger, P. Lodomez, and N. Wermes: (2006). Nucl. Instrum. Methods Phys. Res., Sect. A **560** (2006) 435. https://doi.org/10.1016/j.nima.2006.01.072
17 J. C. Kim, S. E. Anderson, W. Kaye, S. J. Kaye, Y. Zhu, F. Zhang, and Z. He: IEEE Nucl. Sci. Conf. R (2009) 1640–1646. https://doi.org/10.1109/NSSMIC.2009.5402243
18 H. Toyama, A. Higa, M. Yamazato, T. Maehama, R. Ohno, and M. Toguchi: Jpn. J. Appl. Phys. **45** (2006) https://doi.org/8842.10.1143/JJAP.45.8842